

Hardware in the Loop Test of an Electric Aircraft Powertrain

Sebastian Mönninghoff, Moritz Scholjegerdes, Kay Hameyer
INSTITUTE OF ELECTRICAL MACHINES RWTH (IEM)

Schinkelstraße 4

52062 Aachen, Germany

Tel: +49 241 80 97648

E-Mail: sebastian.moenninghoff@iem.rwth-aachen.de

URL: <https://www.iem.rwth-aachen.de>

Keywords

«Airplane», «Electrical Machine», «Test Bench», «Modelling»

Abstract

Electric machines are attracting attention as potential alternatives to conventional aircraft powertrains. During the development process of an electric aircraft it is often necessary to test and analyze the entire powertrain or components before all interacting systems are physically available. The function and behavior of subsystems, which interact with the powertrain, have to be emulated at a test bench. The powertrain is subject to varying external conditions during flight, which effect the function of the subsystems. Environmental conditions and the characteristic behavior of the aircraft have to be considered. This paper studies the development of a hardware in the loop test (HIL test), which allows to emulate flight conditions on a test bed during powertrain testing. The HIL test is subsequently implemented and developed for the example of the touring motor glider FVA 30. A duty cycle is derived from an aircraft flight test case and used to simulate the aircraft behavior. The results of the HIL test indicate, that the aircraft will meet the specified flight performance goals, but also hint at high temperatures inside the v-shaped tail section, which requires further study and possibly additional cooling effort.

Introduction

Testing aircraft components prior to full system integration offers the possibility to study aircraft subsystems and their interactions at early design stages. Thereby cost and risks of ground or flight tests can be reduced by identifying design issues early. The HIL test discussed here is developed exemplarily for the touring motor glider FVA 30.

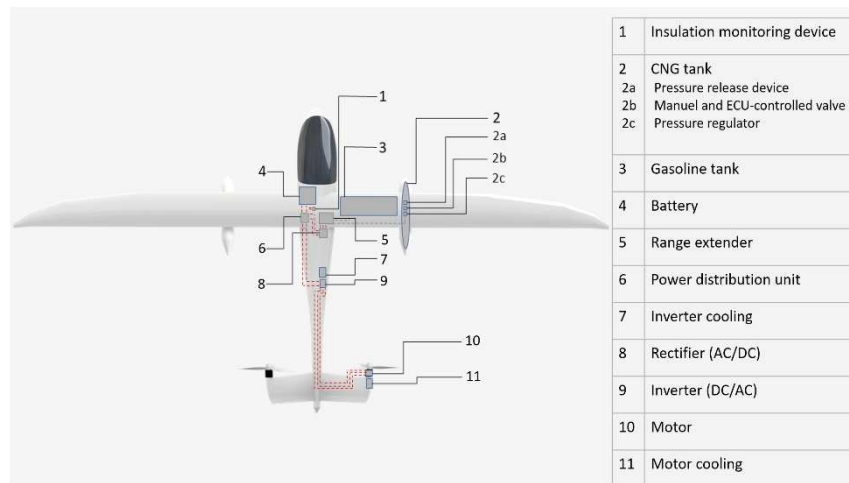


Fig. 1: Components and basic topology of the FVA 30 project [1].

The FVA 30 is a two-seated, hybrid-electric aircraft research platform. It is developed and built by the *Flugwissenschaftliche Vereinigung Aachen (1920) e.V.* (FVA) [1]. The FVA represents an aerospace society, operated and organized by students from RWTH Aachen University. The FVA 30 is based on the motor glider e-Genius of the University of Stuttgart [2]. An overview of the aircraft is shown in figure 1. A particular feature of the FVA 30 is the serial hybrid electric powertrain, which is constructed employing a range extender, a battery, two inverters and two electric machines. The electric machines are mounted to the tips of the v-shaped tail section and are fed by inverters, which are located in the middle section of the aircraft. The FVA has developed the necessary modifications to the structure.

As a constructive boundary condition, the range extender has to be able to run on both, natural gas as well as on gasoline. For this purpose, the natural gas is stored in high-pressure tanks inside the wing pods. The gasoline is stored in integral tanks inside the wings. The combined use of the range extender and the battery enables a range of 650 km. The take-off can be performed without using the range extender, since the aircraft is capable of climbing 1000 m while providing full power to the electric powertrain for 15 minutes by using the battery. [1]

Topology of the HIL Test

The components, which are physically available for the HIL test, include one electric machine, one power electronic inverter, the power cables and a mockup of one tail section side. The measurement campaign includes duty cycle tests, thermal tests, validation of the wiring concept and the prediction of flight performance. During flight operation, the powertrain is subject to varying external conditions, which have to be considered while conducting the tests. Since the inverters, the electric machines and their electric connections are redundant and symmetric, only one side of the powertrain is physically tested at the test bench. The second side of the electric powertrain is accounted for by assuming, that both sides of the powertrain exhibit identical behavior.

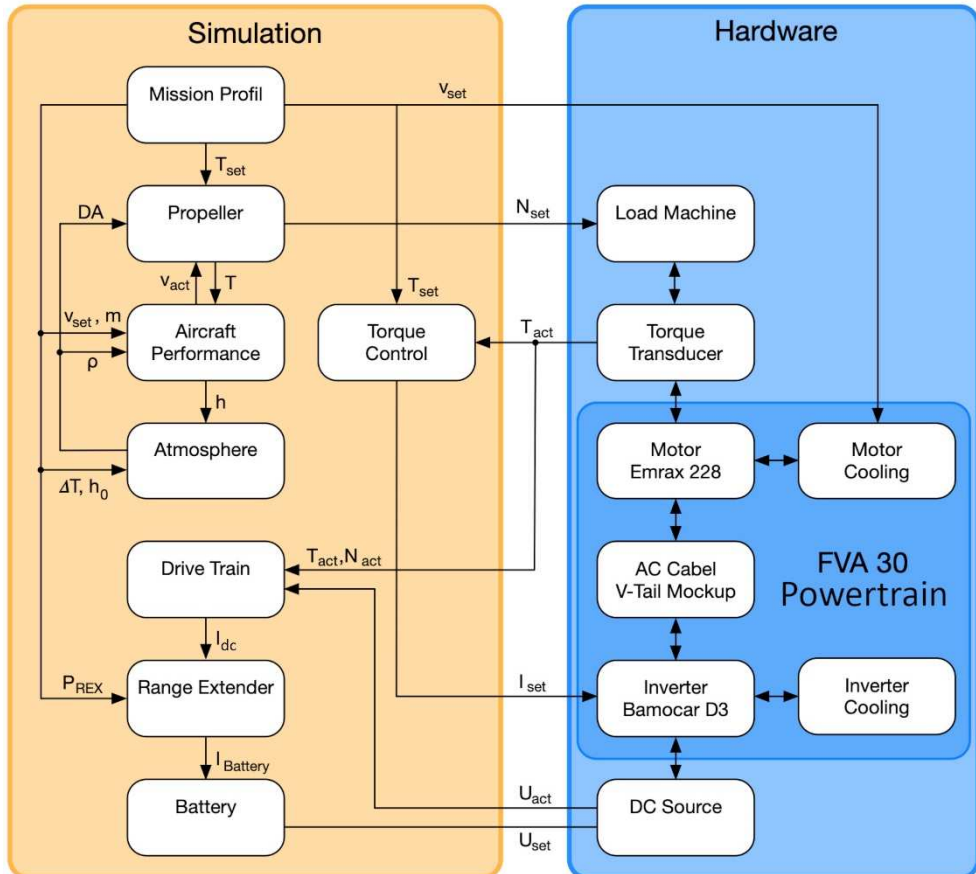


Fig. 2: Topology of the HIL test.

In [3] a framework is proposed, which allows the SIL/HIL testing of aircraft hard- and software components, which are either physically available or simulated. The framework in [3] uses an unmanned aerial vehicle as a test case and the simulator X-Plane to model the aircraft's aerodynamic state. The HIL test proposed in this paper implements a flight performance module directly, which makes use of available measurements of aircraft polars. The atmosphere model allows to simulate environmental conditions encountered during flight. Furthermore the HIL test proposed in this paper focuses on thermal validation of the powertrain concept of a manned aircraft. Cooling systems of the inverter and the electric machine are taken into account and modelled at the test bench. The battery temperature is simulated in the scope of this work, since it is not available physically.

The simulated data can be used to emulate the physical interfaces of the HIL test. A topology for the HIL test is proposed as shown in figure 2. The emulated physical interfaces are the shaft load, the electric connection between the inverter and the battery, the control bus of the inverter and the cooling system of all components.

To emulate the load of the shaft mechanically, an electric machine is employed. The battery behavior is emulated by a dc source, while the control bus of the inverter receives input data from the control hardware at the test bench. The cooling air flow at the test bench is emulated by fans. A mission profile as a duty cycle, is used to set the desired torque and the power provided by the range extender at multiple operating points. All of the aforementioned systems have to be controlled by the HIL test's control hardware to dynamically emulate the physical interfaces in real-time according to the current state of the virtual aircraft.

Physical Interface: Shaft

The proposed HIL test uses the torque T , defined by a mission profile, the state of the aircraft and the atmospheric conditions to calculate a resulting rotational speed of the propeller. Due to operational safety considerations the load machine controls the rotational speed of the HIL test, while the electric machine under test controls the torque.

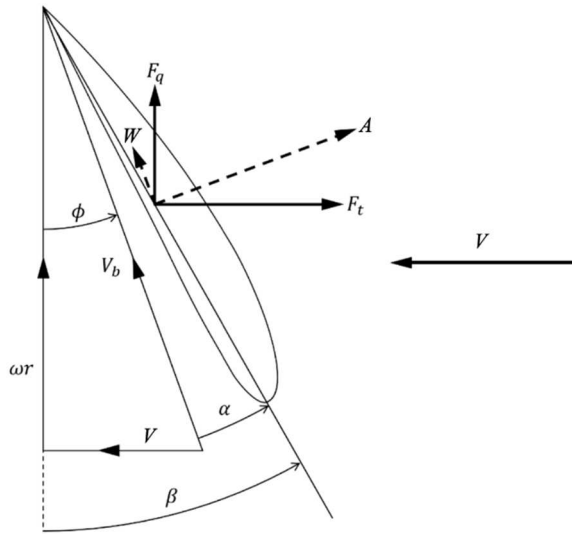


Fig. 3: Forces and velocities at propeller. [4]

The propeller converts the mechanical power of the electric machine into a propulsive force. A propeller has one or more blades rotating around the propeller axis. According to [4] the propeller blades act similar to an airfoil. The airfoils are provided with airflow with the velocity v_b and thus generate lift A and drag W as shown in figure 3. A and W can be transformed into the thrust force F_T and the force F_Q . F_Q results in a drag torque. The resulting blade airspeed v_b is calculated from the aircraft airspeed v_∞ , the radius r and the angular frequency ω with equation 1 according to [4].

$$v_b = \sqrt{v_\infty^2 + (\omega * r)^2} \quad (1)$$

The simulation of the propeller is implemented with precomputed maps to determine rotational speed, thrust and efficiency in real-time. The maps are created for multiple operating points of the propeller, which is modelled with the blade element momentum theory [4], [5]. The propeller module receives a desired torque T_{Set} , the current airspeed of the aircraft v_{act} and the density altitude DA as inputs. The resulting rotational speed N is determined by the precomputed lookup tables. The desired torque T_{Set} is defined by the mission profile, while the current airspeed v_{act} is provided by the aircraft performance model. The air density has to be considered, when determining the current state of the propeller. It is provided as the density altitude DA by the atmosphere model.

The flight performance module is used to calculate the airspeed v_{act} and the altitude h of the aircraft in real-time. Figure 4 shows the forces acting on an aircraft during flight. According to [6] three coordinate systems are used to describe the state of the aircraft. In the aerodynamic coordinate system, the axis x_a is aligned with the direction of the aircraft airspeed vector v . In the geodetic coordinate system, the perpendicular axis z_g is parallel to the gravitational vector. The aircraft fixed coordinate system is bound to the aircraft geometry.

The lift force A acts in the opposite direction of z_a and the drag force W acts in the opposite direction of x_a in the aerodynamic coordinate system. The weight force G acts along the gravitational vector z_g in the geodetic coordinate system. As a simplification, it is assumed that the propeller thrust T is aligned parallel to x_a in the aerodynamic coordinate system. The flight performance module receives the thrust of the propeller F , the density of the surrounding air ρ , the desired airspeed v_{set} and the current aircraft mass m as input.

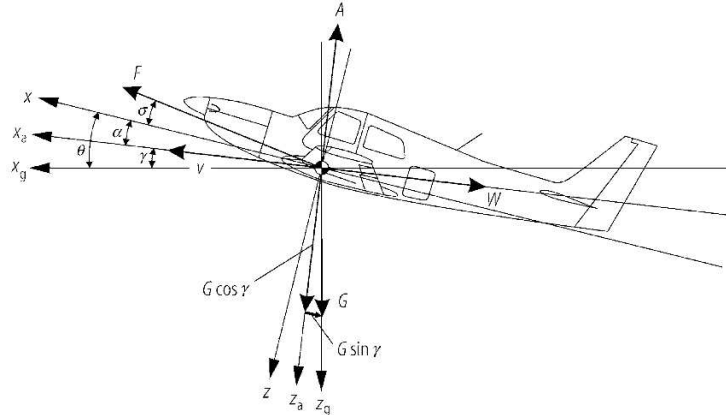


Fig. 4: Angles and Forces acting on an aircraft. [6]

$$0 = A - G * \cos(\gamma) \quad (2)$$

$$0 = F - W - G * \sin(\gamma) \quad (3)$$

$$\gamma = \arcsin\left(\frac{v}{w}\right) \quad (4)$$

In a quasi-stationary flight state without acceleration, a balance of forces is assumed. The relation between the lift A and the weight force G can be described with the equation 2, [6]. The weight force G results from the aircraft mass m and the gravity g . The relation between thrust F , drag W and weight force G is given by equation 3. Aircraft lift and weight are described by coefficients, which are known from measurements of the e-Genius prototype. The thrust is provided by the propeller model. The trajectory angle γ can be determined by the airspeed v and the vertical speed w with equation 4. [4].

The flight attitude control controls the virtual aircraft around the lateral axis. Two PID controllers are used. The first controller controls the climb angle γ over the load multiple n within the limits 0.9 to 1.18. During take-off, n is set to 1 until the rotation speed is reached. The target value for the angle of climb

γ_{set} is calculated with the equation 5 from the thrust F and the drag W_{set} , which would result in a stationary flight state ($n = 1$) at the desired airspeed v_{set} [4].

$$\gamma_{set} = \arcsin\left(\frac{F - W_{set}}{G}\right) \quad (5)$$

The second PID controller uses the airspeed v as reference variable and a difference to γ_{set} as controlled variable. This design allows the speed to be controlled and also limits both n and γ to realistic values. The aircraft performance model and the propeller model depend on atmospheric conditions. The international standard atmosphere (ISA) standardizes these conditions. The basis of the ISA atmosphere is defined at a height of 0 m above mean sea level. The air is assumed to have a standardized temperature of 15 °C, an air density of 1.225 kg/m³ and a pressure of 1013.25 hPa in this height [7].

The international standard atmosphere distinguishes between the air layers troposphere, tropopause and stratosphere [7]. For small aircraft such as the FVA-30 without pressurized cabin, generally only flight altitudes of about 3000 m are permitted without additional oxygen [8]. It is thus further assumed, that all flights take place in the troposphere, which reaches up to an altitude of 11000 m. The flight altitude above mean sea level is converted into the density altitude DA. The density altitude corresponds to the theoretical altitude above a pressure level of 1013.25 hPa. Based on the density altitude, the density is then determined by ISA using an interpolated lookup table.

Physical Interface: Battery

The hybrid power supply of the FVA 30 consists of an internal combustion engine, which is used as a range extender and a Lithium-ion battery. The combustion engine is only designed to provide sufficient power for cruising flight. With respect to the weight, this enables a lighter combustion engine with only 25 kW electric output power. The Lithium-ion battery provides the additional power for take-off and climb, but also enables safe take-off and flying without range extender. Here, the battery is designed for an overload output power of up to 95 kW during take-off and 87 kW during climb.

The drivetrain module calculates the total current I_{dc} necessary to provide the torque T . It takes the current voltage of the battery U , the measured rotational speed N and the measured torque T as input. The current I_{dc} is provided by the battery and the range extender. The range extender module calculates the current, which is drawn from the battery $I_{Battery}$ with the range extender power P_{REX} and the total current I_{dc} as input. The output of the battery module is used to set the voltage of the dc source U_{set} . In the context of this work the battery is emulated by a dc Source at the test bench.

The state of charge SOC results from the charge and the capacity of the cell with the equation 6. The charge of the cell Q_C depends on the initial charge $Q_C(t_0)$ and results from the integration of the cell current I_C over time according to equation 7.

$$SOC = \frac{Q_C}{c_c} \quad (6)$$

$$Q_C(t) = Q_C(t_0) + \int_{t_0}^t I_C(t) dt \quad (7)$$

The *Peukert* effect describes the influence of the discharge current on the storage capacity of the battery. In the data sheets of the batteries a nominal capacity C_N is usually given, which can be taken with the corresponding nominal current I_N . Equation 8 can be used to describe the extractable charge Q in dependence of the current I and the Peukert number k . [9]

$$Q = C_N * \left(\frac{I_N}{I}\right)^{k-1} \quad (8)$$

The temperature T_{bat} is obtained by integrating the power dissipation $P_L(t)$ over time, the mass m and the specific heat capacity c_p with equation 9. [10]

$$T_{bat}(t) = T_{bat}(t_0) + \int_{t_0}^t \frac{P_L(t)}{c_p * m} dt \quad (9)$$

Physical Interface: Data Bus

The data bus of the inverter is used to control the electric machine. With the desired torque T_{set} and the measured rotational speed N the initial i_d , i_q -current combination is determined from a lookup table. A PID controller is used within the torque control module depicted in figure 2 to account for the remaining difference between the desired torque and the measured torque. The inverter is controlled via a CAN bus.

Physical Interface: Cooling

The electric machine and the inverter use separate liquid cooling systems. In both cases a pump circulates the coolant through the component and a radiator.

The radiator of the electric machine is installed directly in the nacelle behind the propeller, so that an air flow is provided by the propeller. To emulate an equivalent air flow on the test bench an additional fan is used, which is directly mounted to the radiator as shown in figure 5. The speed of the air flow is measured by anemometer measurements in a circular duct on the suction side of the fan. Due to the known velocity profile of the air flow in the circular duct the mass flow can be calculated. The fan is set to generate the airflow expected during flight operation of the aircraft. The electric machine will be mounted on a steel mount in the aircraft. On the test bench however, the machine is mounted on an aluminum base plate with higher heat conductivity and a test bench mount with higher heat capacity than the real structure. To reduce the influence of the test bench mount on the heat dissipation mechanisms, the contact area between the electric machine and the aluminum plate is designed to be as small as possible. The plate is also insulated by sheets of foam to reduce convection at the plate surface.

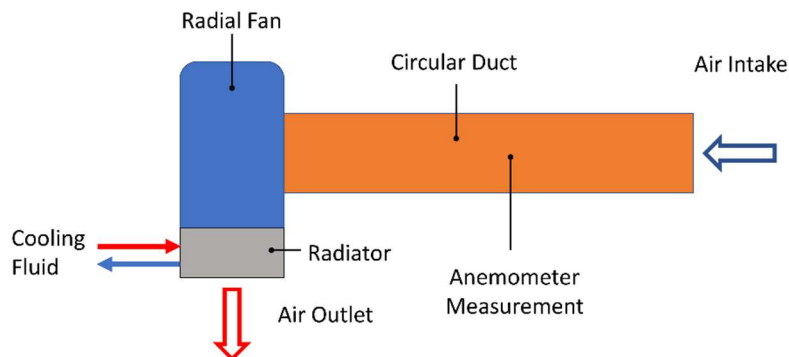


Fig. 5: Cooling setup of electric machine.

The inverter is installed further forward in the fuselage and needs a fan, which ensures sufficient air flow through the inverter radiator even when the aircraft is rolling at low speed. The inverter is equipped with a liquid cooling circuit. On the test bench the same setup is used as in the aircraft according to the current state of the aircraft design. The speed of the fan is fixed.

The cooling of the wiring was identified as a potentially critical aspect during the aircraft design process. Due to the restricted range of the center of gravity of the aircraft the inverters have to be placed beneath the wing section of the aircraft. The two electric machines are mounted on the v-shaped tail section of the aircraft. The electric wiring is routed from beneath the wing section through the whole tail section of the aircraft to the electric machines. Joule losses lead to increased temperatures in the cables and the

surrounding structure. Since there is no airflow available in the aircraft body, natural convection is expected to be the dominant cooling mechanism in the vicinity of the wiring. The surrounding fiber reinforced polymer structure imposes an upper temperature limit of 80 °C on the wiring [11]. The HIL test is set up in such a way, that the wiring can be studied under realistic thermal conditions. A mockup of the v-shaped tail section is used at the test bench to encase the wiring. The upper opening of the mockup is sealed to create worst case conditions with impeded natural convection.

Measurements

Figure 6 shows the setup at the test bench. To emulate the physical interface of the shaft, the electric machine of the FVA 30 is coupled to a load machine with a torque transducer in between the machines. The measured torque and rotational speed are used as input for the HIL test software. The load machine is controlled by the HIL test software to emulate the behavior of the propeller.

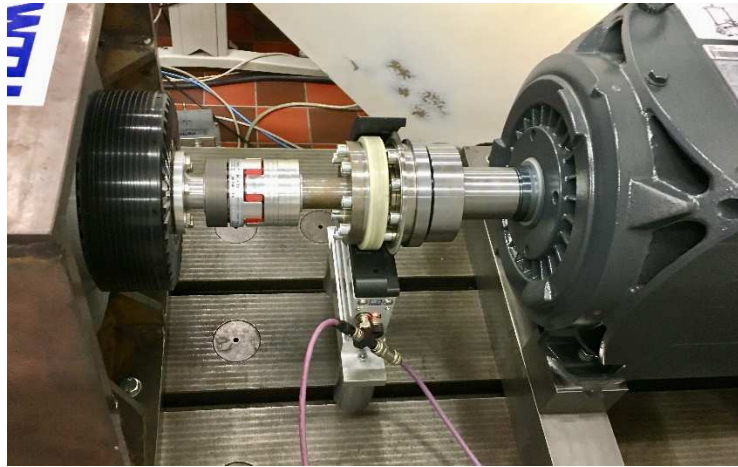


Fig. 6: Mechanical connection of the shaft with torque and speed sensors.

The electric machine of the FVA 30 is supplied by the inverter, which is used in the aircraft, while the load machine is supplied by a test bench inverter. The inverter of the FVA 30 is provided with electric power by a dc source. The inverter current is measured and used as input data for a model, which characterizes the battery. The voltage of the dc source is controlled by this model to simulate the battery behavior.

A mockup of the v-shaped tail section was constructed and equipped with temperature sensors to monitor the temperature in the glass fiber structure of the plane. This setup enables realistic measurements of temperatures occurring during the duty cycle.

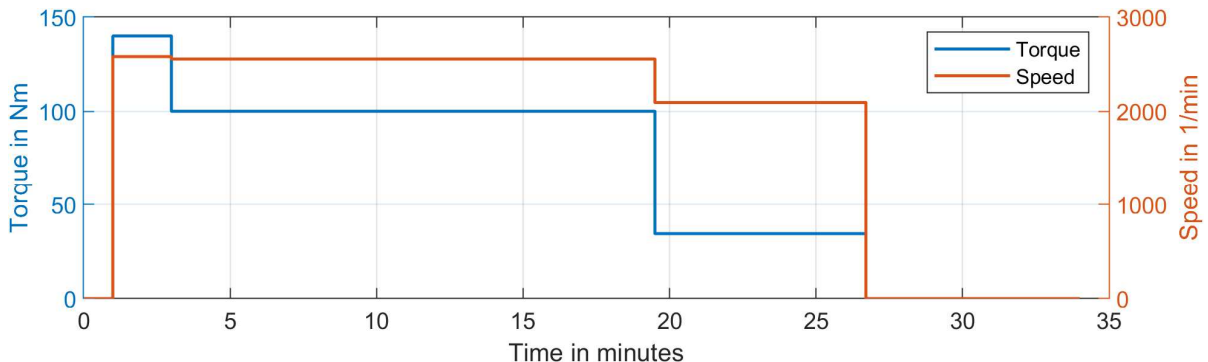


Fig. 7: Assumed duty cycle and operating conditions for the laboratory measurement.

To simulate the maximum expected load on the powertrain, the duty cycle shown in figure 7 is used. It simulates the take-off followed by an ascend until the battery is depleted. The time t_{vl} between the end of the take-off power phase and the arrival at cruise altitude depends on the aircraft simulation and is determined during the test run.

Figure 8 shows component temperatures, which are measured during the test run. The battery temperature is simulated, since it is emulated by a dc source and not physically available. The electric machine's coolant pump is operated at 8.1 l/min and the fan between 360 and 410 m³/h during the tests. During the measurements the ambient temperature is measured at 24 °C, which results in a correction of 14 K to account for the highest expected temperature under real operating conditions. Measurements shown in figure 8 show, that the maximum end-winding temperature of the electric machine is about 74 °C while operated at maximum continuous power. Corrected for warm days this results in 88 °C, which is well below the manufacturer's limit of 120 °C. The electric machine coolant temperature stabilizes at 44 °C.

The coolant pump of the inverter is operated at 7 l/min and the fan between 210 and 250 m³/h during the tests. The temperatures of the inverter IGBTs stabilize at 48 °C, which corresponds to a compensated

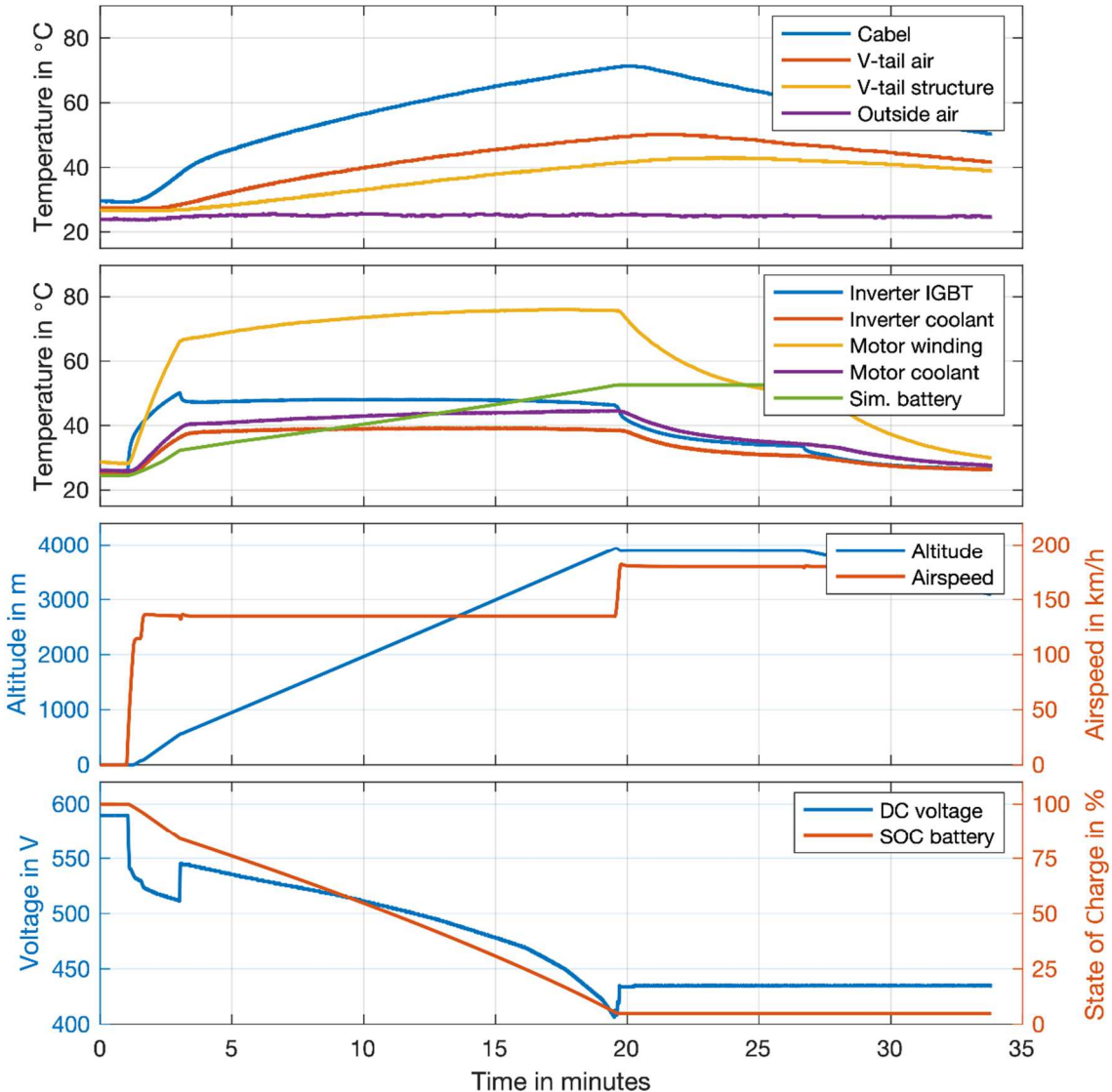


Fig. 8: Temperatures and simulated state of the aircraft.

temperature of 62 °C. This temperature is below the 75 °C of the inverter overtemperature warning. The coolant settles at 39 °C. The corrected temperature of 53 °C is below the 65 °C maximum inlet temperature of the inverter cooler. The air in the tail section reaches a temperature of 52 °C, which corresponds to corrected 66 °C. The actual heating of the tail section's inner side reached its maximum at 43 °C and corrected 57 °C. The material of the tail section has to be heat treated to withstand this temperature [11]. All components in the tail section must be able to withstand the treatment. This should be considered separately during the aircraft design process when selecting materials for the tail section.

During the duty cycle the aircraft is able to ascend to 4000 m above the initial altitude. The simulated state of charge of the battery and the temperatures of all components show, that the electric powertrain design fulfills the requirements set by the duty cycle.

Conclusions

The HIL test proposed and discussed in this paper is implemented at a test bench and used to validate the powertrain design of the FVA 30. The HIL test offers the possibility to test the electric powertrain with realistic duty cycles. The cooling of the components is set up to mimic the situation in the final aircraft design. This enables the determination of the thermal powertrain performance under realistic conditions and the prediction of overall flight performance of the aircraft.

The measurement results show, that the cooling for inverter and electric machine are sufficiently dimensioned. The HIL test is also used to validate the voltage range of the battery. The battery, supported by the range extender, provides sufficient energy to climb to almost 4000 m above the initial altitude. The voltage level is sufficient to achieve the required rotational speed throughout the entire duty cycle.

The HIL test measurement results demonstrate, that the electric losses in the connecting cables lead to increased temperatures in the tail section. The material of the tail section itself is warmed up considerably. In the further design process, these findings have to be considered in the fuselage design, so that an unacceptable temperature increase in the material can be avoided. In further tests the use of an active ventilation of the tail section and its influence on the temperatures could be interesting.

References

- [1] Moxter T., Enders W., Kelm B., Scholjegerdes M., Koch C., Garbade M., Dahmann P.: Investigation of Alternative Propulsion Concepts for Small Aircraft with the Hybrid Electric Motor Glider FVA 30, Proc. Conf. DLRK 2020, 2021.
- [2] Schumann L.: Reduktion des Energiebedarfs mittels eines batterieelektrischen Antriebs am Beispiel eines Kleinflugzeugs, Universität Stuttgart, 2018.
- [3] Bole B., Teubert C., Chi Q.C., Hogge E.: SIL/HIL replication of electric aircraft powertrain dynamics and inner-loop control for V&V of system health management routines, Annual Conference of the PHM Society, 2013.
- [4] Gudmundsson S.: General Aviation Aircraft Design, Applied Methods and Procedures. Butterworth-Heinemann, 2013.
- [5] Glauert H.: The Elements of Aerofoil and Airscrew Theory, Cambridge University Press, 1983.
- [6] Grote K. H., Bender B., Gohlich D.: Dubbel - Taschenbuch für den Maschinenbau. Springer-Verlag, 2018.
- [7] Scheiderer J.: Angewandte Flugleistung: eine Einführung in die operationelle Flugleistung vom Start bis zur Landung. Springer Science and Business Media, 2008.
- [8] Mies J.: AOPA Germany Safety Letter, Sauerstoffmangel, AOPA Germany, 2018.
- [9] Omar N., Daowd M., Bossche P. v. D., Hegazy O., Smekens J., Coosemans T., Mierlo v. J.: Rechargeable energy storage systems for plug-in hybrid electric vehicles-Assessment of electrical characteristics. Energies, 5(8), 2012.
- [10] VDI-Gesellschaft Verfahrenstechnik und Chemieingenieurwesen: VDI-Wärmeatlas. Springer Vieweg, 2013.
- [11] Hexion, Specialty Chemicals, Epoxy and Phenolic Resins Division Epoxy Resins: EPIKOTE Resin MGS LR 285, 2010.